Electrical Power and Energy Systems 126 (2021) 106600

Contents lists available at ScienceDirect

International Journal of Electrical Power and Energy Systems

journal homepage: www.elsevier.com/locate/ijepes

Study of DC partial discharge on dielectric surfaces: Mechanism, patterns and similarities to AC

Saliha Abdul Madhar [a,b,*], Armando Rodrigo Mor [a], Petr Mraz [b], Rob Ross [a]

[a] Delft University of Technology, Mekelweg 4, 2628 CD Delft, the Netherlands
[b] Haefely AG, Birsstrasse 300, 4052 Basel, Switzerland

ARTICLE INFO

Keywords:
Partial Discharge (PD)
HVDC
Pulse Sequence Analysis (PSA)
Material properties
Surface discharge
Pattern recognition

ABSTRACT

This paper presents the investigation on surface discharge behavior of various dielectric samples under DC. It sequentially develops the knowledge base for the study and analysis of the partial discharge (PD) defect with the goal of PD defect identification under DC. In order to facilitate this, the material properties of the dielectric are measured. Finite Element (FEM) simulation is used to obtain the preliminary estimates of the electric field and dielectric properties that concern partial discharge behavior. The DC-PD tests performed on the surface dielectric samples demonstrate a highly plausible behavior based on simulation results and other literature. It also displays a great degree of similarity towards the AC surface discharge behavior. The paper concludes by presenting novel partial discharge fingerprints for the surface PD defect that will aid in defect identification under HVDC.

1. Introduction

AS the power rating of the transmission network increases and the system moves from high voltage (HV) to extra high voltage (EHV) and ultra-high voltage (UHV), the criticality of the network elements also has been increasing. This has given rise to an expectation of increased level of reliability when it comes to asset quality. Each component of the power system, such as cables, bushings, transformers, Gas Insulated Switchgears (GIS) etc., are all tested for insulation defects before and after commissioning. With the traditional power grid designed for AC operation, partial discharge (PD) testing established itself as one of the most powerful and insightful tools in defect elimination and quality assurance. PD testing become a vital tool in all stages of the asset life-cycle such as design, production, commissioning, monitoring/maintenance and diagnostics. However, the recent trends in HVDC with the introduction of long-haul DC lines along with its associated infrastructure have introduced additional concerns if not problems. The insulation system so far employed for AC is known to behave differently under DC stress conditions. The design of DC applications is a challenging process, the electric field calculations are made taking in account its dependence on operational temperature and changes in electrical conductivity of the respective insulating media [1]. Likewise, various other effects such as charge trapping, homo/hetero charge formation at interfaces and irregularities have made the realization of robust DC components a highly sophisticated process [2]. Due to these complexities, the partial discharge behavior of the insulation in the presence of various defects also remains highly elusive and distinct from the AC discharge behavior.

This research is a part of a series investigating the various popular defect types that occur on insulation system, understanding their underlying mechanism and providing patterns that will aid in their identification. This particular paper investigates the surface defect model, which is a common PD source in insulation system, occurring over dielectric interfaces, sometimes also referred to as creping discharge. These kinds of discharges occur on gas–solid interfaces and deteriorate the insulation over time. There are visual Phase Resolved PD (PRPD) patterns to recognize these kinds of defects under AC voltage stress. In this contribution, the discharge mechanism and patterns of a surface defect model under DC stress are studied and presented.

The paper is organized in the following manner: Section 2 presents the relevant electrical properties of the dielectrics under study. In section 3, the simulation results of the surface discharge model under DC voltage are described. The results and observations of the AC and DC-PD tests, the obtained discharge patterns and inferences are discussed in Section 4. The last section is committed to presenting the striking similarities between the AC and DC discharge processes.

* Corresponding author.
E-mail addresses: S.AbdulMadhar@tudelft.nl (S. Abdul Madhar), A.RodrioMor@tudelft.nl (A. Rodrigo Mor), pmraz@haefely.com (P. Mraz), Rob.Ross@tudelft.nl (R. Ross).

https://doi.org/10.1016/j.ijepes.2020.106600
Received 17 August 2020; Received in revised form 29 September 2020; Accepted 19 October 2020
Available online 16 November 2020

2. Electrical properties of the dielectric

The measurement of electrical properties of the dielectric samples is essential for the study of partial discharges in order to understand the underlying discharge mechanisms. The measured electrical properties also serve as a basis for the simulations performed in the following section. Therefore, this section presents the results of the measured electrical conductivity and dielectric constant of the samples investigated. The dielectric constants of the insulating samples are measured using the Tettex 2830 dielectric analyzer together with the Tettex 2914 test cell for solid insulants. The measurement of volumetric and surface dielectric properties is done according to the standard IEC 62631-3-1 and 62631-3-2 respectively [3,4], details of the measurement setup and technical specifications are presented in [5]. The measurement principle is based on a 3-electrode system consisting of namely, 1: main (HV) electrode, 2: measuring electrode and 3: guard electrode as shown in Fig. 1. The relative permittivity (ε_r) is measured at AC power frequency (50 Hz) directly based on Eq. (1).

$$C = \frac{\varepsilon_r \varepsilon_o S}{h} = C_o \varepsilon_r \tag{1}$$

Where ε_o is the permittivity in free space, C is the measured capacitance of the sample, S is the effective surface area of the measuring electrode and h is the thickness of the sample.

The DC tests are carried out to measure the volume and surface resistivities of the dielectric samples. The volume resistivity (ρ_v) of the sample is measured in the electrode arrangement shown in Fig. 1 and derived from the value of measured resistance (R_s) using the relation shown in Eq. (2).

$$\rho_v = \frac{R_s S}{h} \tag{2}$$

Where S is the effective surface area of the measuring electrode and h is the thickness of the sample. It becomes highly challenging to measure the resistivities of samples with high resistivity (or thick samples $>$ 3 mm). The surface resistance values of dielectric samples are measured using a similar 3-electrode setup as for measurement of volume properties, however, with the reversal of the HV and guard electrodes. The current flowing in the annular ring is measured and the surface resistivity, ρ_s, is deduced using the expression given by Eq. (3).

$$\rho_s = \frac{d_2 + d_1}{d_2 - d_1} \pi . R_s \tag{3}$$

Where R_s is the measured resistance, d_1 is the diameter of the inner electrode and d_2 is the inner diameter of the ring electrode. In order to get the absolute value of surface conductivity without the influence of the air gap, a special Teflon ring was manufactured and fitted in the gap. This explains the high values of surface resistivity presented in Table 1.

Four different samples were studied as a part of the surface discharge study. Samples A and B were dielectrics used in power cable application, sample A developed for high voltage applications and sample B for low voltage applications. Sample C was a high-grade Teflon commonly used in high voltage constructions and sample D a resin impregnated pressboard commonly used in transformer constructions. The results of the measurement are presented in Table 1. The dielectric constant of the samples A, B and C lie in the range of 1.5–2.2 which is commonly the expected range for Polyethylene and Teflon. The dielectric constant for sample D however is relatively high compared to the other samples. This is because the resin impregnated pressboard is designed for operation in oil and when not immersed in oil, the pressboard sample contains traces of moisture that results in a high value of ε_r. Based on the results of the measured volumetric electrical resistivity, the samples can be broadly classified into high and low resistive samples. While sample A and C are highly resistive with resistivities in the range of a few PΩm, Sample B and D are poorly/low resistive. Sample D has the lowest resistivity with a value of 2.14 GΩm while sample B has a resistivity of 24 TΩm (see Table 1).

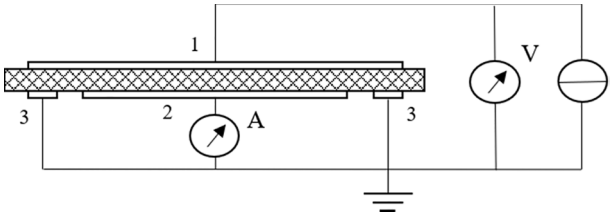

Fig. 1. The circuit schematic for measurement of volumetric dielectric properties based on IEC 62631-3-1[3].

Table 1
Results of the measurement of dielectric properties of the samples under study.

Sample identifier	ThicknessH [mm]	Dielectric constant ε_r	Volume resistivity (ρ_v)[TΩm]	Surface resistivity (ρ_s) [TΩm]
A	0.58	2.18	2.98×10^3	6.91×10^4
B	2	1.57	2.4×10^1	1.04×10^4
C	0.6	1.95	6.4×10^3	6.91×10^4
D	3	8.0	2.14×10^{-3}	1.04

The surface resistivity is associated with the resistance over surface tangent or the horizontal axis of the material. This measured value is extremely high for samples A and C where the maximum measuring limit of the device is reached. The other measured values for samples B and D are listed on Table1. The implications of this variation in electrical properties is investigated through FEM simulation in the next section of the paper.

3. Simulation of the surface discharge model

The use of simulation in this study was to derive the first estimates of the DC field stress and understand the influence of and the interaction between dielectric properties of interfacial media. This was done using the COMSOL® Multiphysics user software which works based on Finite element method (FEM) by solving Partial Differential Equations (PDE). The following sections describe the setup, results and observations in greater detail.

3.1. Model setup

A concentric electrode arrangement is used for the simulation model with high voltage applied to the center electrode and the peripheral electrode at ground potential. The lower electrode on which the dielectric sample is placed is also at ground potential. This arrangement is chosen in order to enhance the tangential field stress over the dielectric surface that cause the surface discharges. The arrangement is placed in infinite medium of air using the infinite element domain available on COMSOL. The properties of the different media are listed in Table 2. A dielectric constant of 2.3 which is in the range of the dielectric constant of organic dielectrics like polyethylene and Teflon is used in the simulation. In case of DC simulations, the electrical conductivity of the sample is specially modelled as a function of temperature and electrical field stress, σ(T,E). The dimensions of the arrangement can be estimated

Table 2
Material properties used in the simulation.

Medium	Material properties	
Electrodes	Aluminum 3003-H18 (built-in)	
Surrounding medium	Air (built-in)	
	Electrical conductivity (S/m)	$1 \times 10^{-13}$to 1×10^{-9}
Sample/substrate	Dielectric sample	
	Relative permittivity	2.3
	Electrical conductivity (S/m)	σ(T,E)

from Fig. 2. A dielectric sample with thickness 1 mm is used for the purpose of simulation.

The model is studied under both AC and DC electrical stresses. The AC simulation is accomplished through the electrostatic physics and a steady-state study [6]. An electric potential of 10 kV is applied to the HV electrode. This value represents the maximum value of AC voltage and not the RMS (root mean square).

The DC simulations are implemented using the electrical currents physics interface and a time dependent study. An electrical potential of the same 10 kV is applied to the HV electrode. The time dependent study is solved for steps of 10 ms, starting from 10 ms until 1 s. The major difference between the AC simulation implemented using the electrostatics physics interface and the DC simulation using the electrical current interface is the manner in which the electrical fields are deduced. In the AC case, the electrical fields are solved based on the gauss's law;

$$\nabla . D = \delta_v \; D = \varepsilon E \tag{4}$$

Where, D is the electrical flux density in C/m^2, E is the electrical field intensity in V/m, ε is the permittivity and δ_v is the volume space charge, if present. In the absence of space charge the Poisson's equation $\nabla^2 V = -\delta/\varepsilon$ is reduced to zero based on the relation of electric field derived from the gradient of voltage, $E = -\nabla V$. Therefore, the pre-requisites for the prediction of electric field strengths over a given geometry under AC voltage is the permittivity of the dielectric (ε_r, $\varepsilon = \varepsilon_0 \varepsilon_r$) and the values of electrical potential (V).

In case of DC, the electrical currents physics interface solves for the equation of current continuity derived from the Ampere-Maxwell's law;

$$J = \sigma E + \frac{\partial D}{\partial t} \tag{5}$$

$$\nabla . J = Q_v \tag{6}$$

Where, J is the current density in A/m^3, σ is the electrical conductivity in S/m and Q_v the resultant charge density in C/m^3. The first term to the right in Eq. (5) depicts the conductive current, while the second term represents the displacement current as a result of the rate of change of the electrical flux density. The pre-requisites for the implementation of a time-domain study for DC field estimation are the values of electrical conductivity (σ) and the electric potential (V). The electrical conductivity for the dielectric medium is implemented based on Eq. (7), in order to incorporate its dependency on temperature and electric field stress [1].

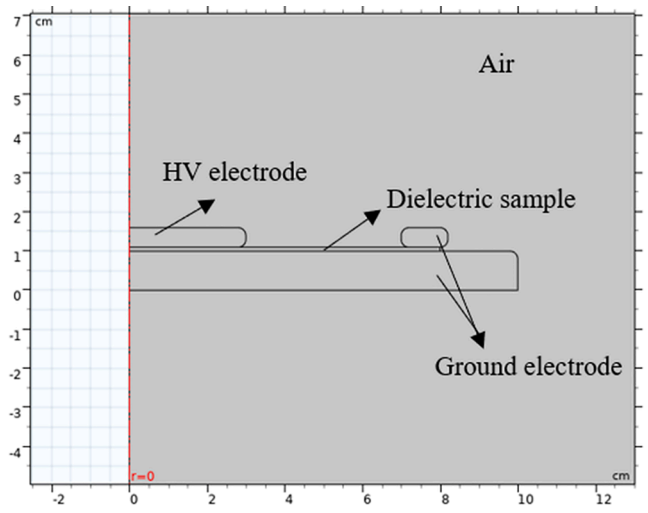

Fig. 2. Geometry of the surface discharge model setup in COMSOL Multiphysics.

$$\sigma(T,E) = A.\exp\left(\frac{-0.98q}{K_B T}\right) \frac{\sinh\left(2.7755 \times 10^{-7} \times |E|\right)}{|E|} \tag{7}$$

Where, A is a variable value in the range of 3.2781×10^{11} that can be tuned to obtained the desired range of conductivity, T is the temperature in K, q is the value of elementary charge equal to 1.6×10^{-19} C and K_B is the Boltzmann constant equal to 1.38×10^{-23} m^2 kg s^{-2} K^{-1}.

3.2. Results and observation

The resultant values of tangential electrical field stress along the air-dielectric interface is shown in Fig. 3. Fig. 3(a) gives the AC field distribution. It can be observed that the electrical field reaches a maximum value close to the triple-point (electrode-air-dielectric) which causes the local breakdown of the dielectric interface, producing surface PD.

The same arrangement is simulated for the DC case with the electrical conductivity of the dielectric (sample) implemented based on Eq.

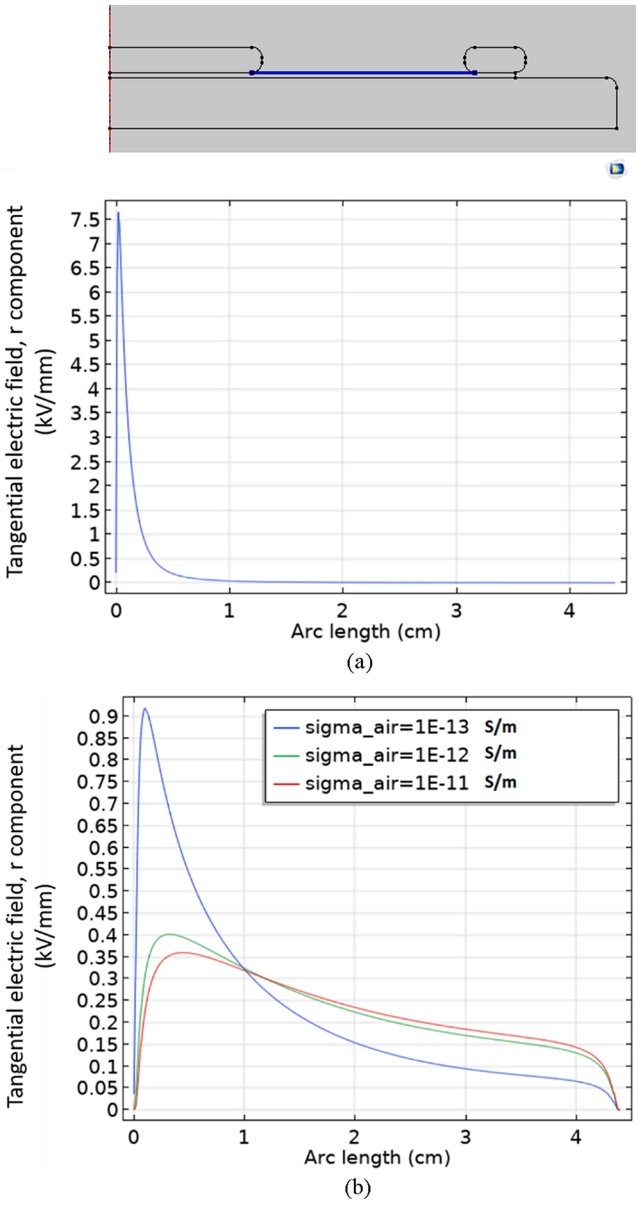

Fig. 3. Plot of tangential electrical field along the dielectric interface (highlighted in the image above) under (a) AC and (b) DC voltage stress conditions for sample conductivity, $\sigma_d = 5 \times 10^{-15}$ S/m and air conductivity as indicated on figure label.

(7). The sample's dielectric conductivity is chosen based on the maximum and minimum measured values presented in section 2 and based on this four different combinations/cases are simulated as listed on Table 3. For case I, II and III the sample's electrical conductivity (volumetric) is chosen to be in the range of 5×10^{-15} S/m and the electrical conductivity of the surrounding air medium is changed using the parameter sweep feature in COMSOL. The conductivity of air varies over a wide range between 10^{-13} to 10^{-9} S/m based on the location, humidity, composition and several other variables [7]. The DC field in Fig. 3(b) is simulated for three cases of $\sigma_{air} = \left[10^{-13}, 10^{-12}, 10^{-11}\right]$ S/m. The results presented are all at steady state when the electrical field reaches the stable DC field distribution. And the DC field distribution can be determined by plotting the field transition over time. Fig. 4 demonstrates this process by plotting the transition of the electrical field from capacitive to resistive field for case II. Alternatively, it is also possible to plot the maximum of the tangential field component over the dielectric interface as a function of time to observe the change. This is shown in Fig. 5 where the field value reaches steady state around 1000 s.

A stark contrast is observed in the electrical field distribution over the dielectric surface in the AC and DC cases. For the given simulated configuration, the DC field distribution shows a much softer peak around the triple-point and a much elevated field stress close to the ground electrode with respect to the AC case. Additionally, along with the results of the surface charge distribution for the respective cases (I, II and III) presented in Fig. 6, the following observations can be made:

- Lower the disparity in the resistivities of the two media (air and solid), lower is the surface charge accumulation.
- The electrical field along the interface increases with increasing the resistivity of the surrounding air media (reducing the disparity between the resistivities of the two media).

In other words, the extreme differences in resistivities of the interfacial media lead to charge retention on the dielectric surface which in turns opposes the applied electrical field and lowers the tangential electrical field stress which is the cause of the surface PD. An additional inference could be made regarding the time taken to reach steady state/DC field distribution. High surface resistivities lead to large RC constants and hence longer time to DC resistive fields. This parameter gives very useful information regarding the waiting time (also known as charging time).

Case IV involves the simulation of a dielectric with higher electrical conductivity ($\sigma_d = 5 \times 10^{-12}$ S/m and $\sigma_{air} = 10^{-11}$ S/m) to demonstrate the lowered waiting times. The resultant electrical field stress and the

Table 3
Simulation results of the surface discharge model under DC field conditions.

Electrical conductivity of Air(σ_{air}) in S/m	Electrical conductivity of dielectric sample(σ_d) in S/m	Max. tangential electrical field stress(E_{tan}) in kV/mm	Max. surface charge density at 10 mm (arc length) in nC/cm^2	Approximate time to steady state
Increasing the resistivity of surrounding air medium with high resistive sample:				
Case I: 1×10^{-11}	5×10^{-15}	0.36	14	~ 4 s
Case II: 1×10^{-12}	5×10^{-15}	0.4	13.3	~ 16 min
Case III: 1×10^{-13}	5×10^{-15}	0.92	9	~ 1 h 40 min
Low resistivity of surrounding air with low resistive sample:				
Case IV: 1×10^{-11}	5×10^{-12}	3.6	2.1	~ 15 s

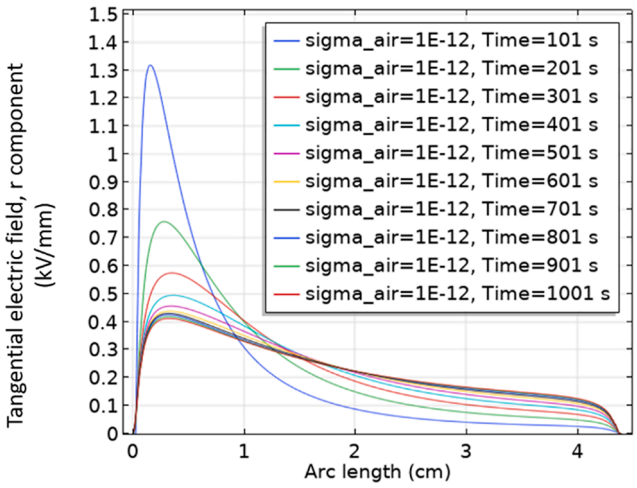

Fig. 4. Tangential electrical field distribution plotted along the dielectric interface with sample conductivity, $\sigma_d = 5 \times 10^{-15}$ S/m and air conductivity $\sigma_{air} = 1 \times 10^{-12}$ S/m under DC stress at specified time instances.

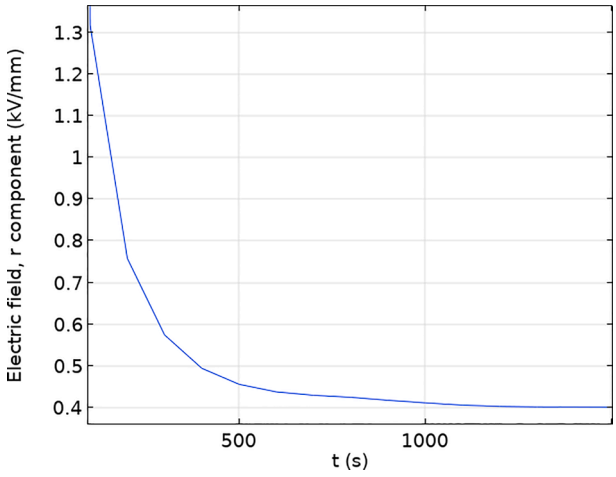

Fig. 5. The maximum value of tangential electrical field component over the dielectric interface with sample conductivity, $\sigma_d = 5 \times 10^{-15}$ S/m and air conductivity $\sigma_{air} = 1 \times 10^{-12}$ plotted as a function of time.

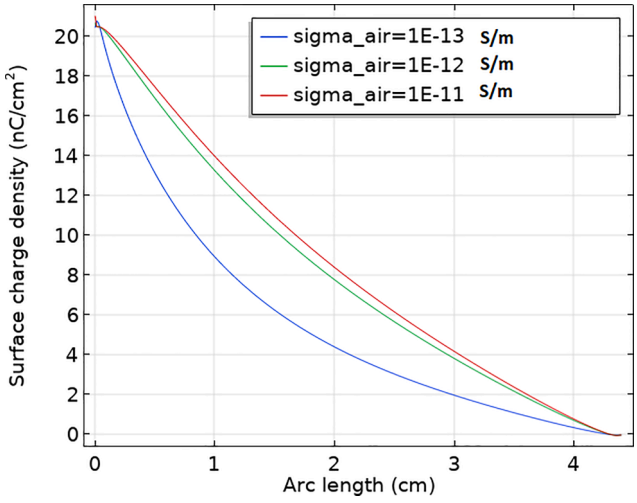

Fig. 6. Plot of surface charge density on the air-dielectric interface under DC stress conditions for sample resistivity, $\sigma_d = 5 \times 10^{-15}$ S/m.

surface charge density are presented in Fig. 7 and Fig. 8 respectively.

It can be observed that the tangential electrical field over the air-dielectric interface has predominantly increased (x4) and the distribution now resembles closely the AC field distribution though the intensity is still half that of the AC case. Nevertheless, unlike Case III, the time to DC steady state is now lowered as expected due to the smaller RC time constant.

4. AC and DC surface discharge testing

The surface discharge tests are carried out under both AC and DC (positive and negative polarity) voltage stress. The defect arrangement used for both cases remains the same while the measuring circuit is modified as described in Section 4.1. The following subsections describe the results and observations of the tests.

4.1. Experimental setup

The surface discharge model is implemented as a sandwich model with the dielectric sample (under test) held securely between two electrodes. The schematic of the defect arrangement is shown in Fig. 9. Voltage is applied to the upper electrode while the lower electrode is at ground potential. In order to ensure there are no air gaps between the HV electrode (upper electrode) and the sample, a spring system is used on the upper suspender. The lower electrode is maintained to be of dimensions larger than the dielectric sample with the aim of creating a singular dielectric interface for the surface discharge activity. The dielectric samples are cleaned with alcohol and cellulose-free paper before testing. The dimensions relating to the thickness of the sample, mentioned to be ~ 2 mm on Fig. 9 is only an estimate. The actual thickness is variable for different dielectric samples and varies between 0.5 and 3 mm.

The AC measuring circuit has been implemented based on the IEC standard 60270 as shown in Fig. 10 [8]. A PD free high voltage AC source is chosen for the test. A coupling capacitor in series with a measuring impedance (Z_m) is connected in parallel with the defect arrangement. The connections are kept low inductive, as the PD pulse is a high frequency pulse. All components of the measuring setup, excluding the defect are ensured to be PD free in the test voltage range. The PD detector, DDX 9121b is used as the front end of the measurement. It logs the values of voltage, charge (pC), repetition rate and pulse polarity every second, providing a real time estimate of the PD events. The signal output channel over its front panel of the DDX provides the possibility of streaming the PD raw data using an external oscilloscope.

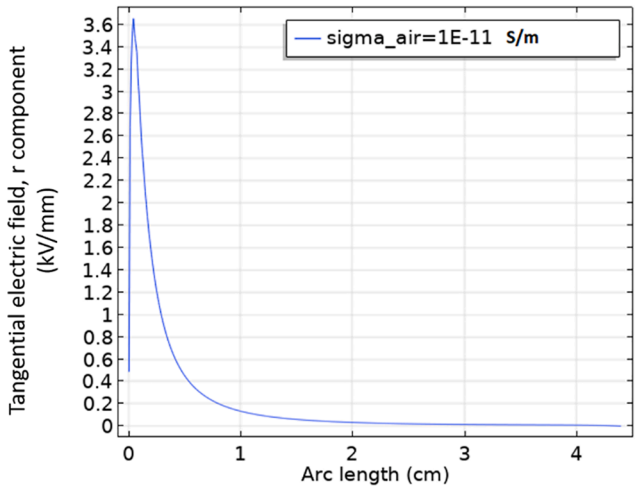

Fig. 7. Plot of tangential electrical field along the air-dielectric interface under DC voltage stress conditions for low resistive sample.

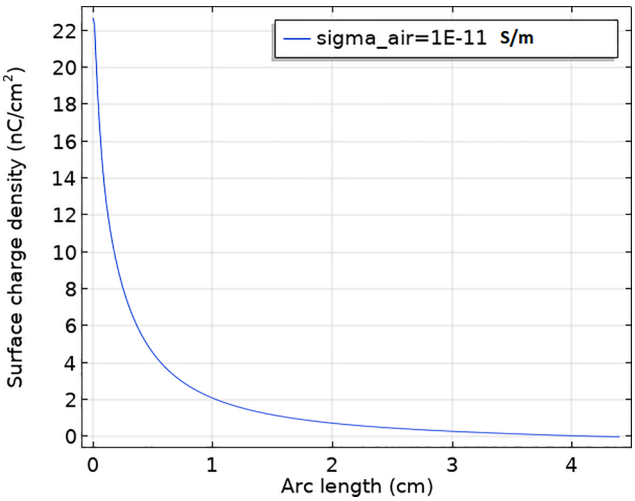

Fig. 8. Plot of surface charge density over the air-dielectric interface under DC stress conditions for low resistive sample.

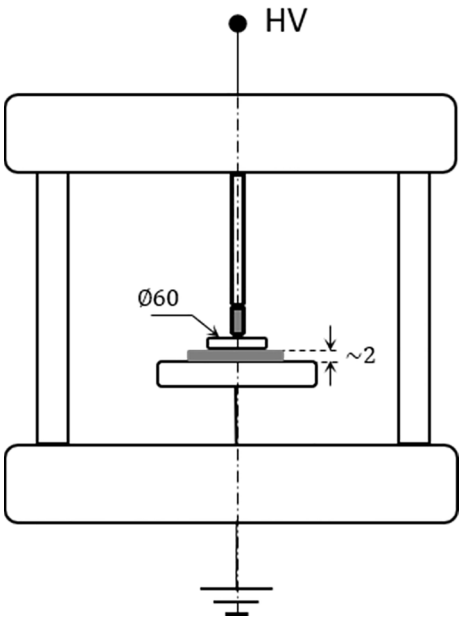

Fig. 9. Schematic of the surface discharge defect arrangement (all dimensions are in mm).

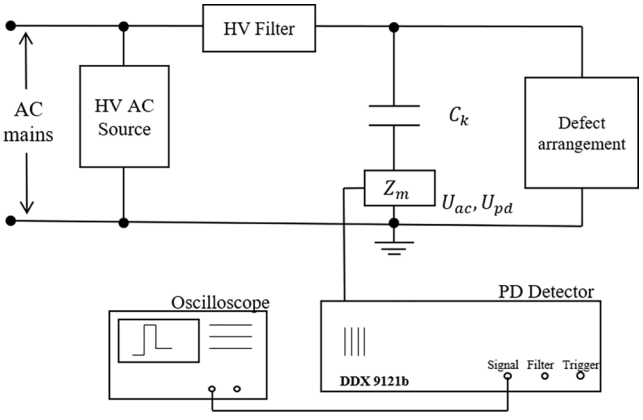

Fig. 10. Schematic of the AC-PD measuring setup according to IEC 60270 [8].

An external oscilloscope with a measuring bandwidth (BW) of 250 MHz is used for streaming the PD raw data at a rate of 10 or 20 MS/s. The PD raw data once recorded is post-processed through a special set of algorithms developed on MATLAB software.

The DC measuring setup is shown in Fig. 11, it employs a half-wave rectifier circuit with a large smoothing capacitor in order have minimum voltage ripple. The value of the smoothing capacitor in this case is 25 nF. Due to the large value of the smoothing capacitor it becomes imperative to use a good HV filter (mostly an inductive coil with a low resistance, represented by L_b on Fig. 11) in order to have a good PD measuring sensitivity. A R||C voltage divider in parallel with the defect arrangement is used to measure the applied DC voltage. The measuring chain involving the measuring impedance, the PD detector and the oscilloscope is maintained similar to the AC case.

4.2. AC test: results and observations

The AC-PD tests are carried out prior to the DC tests to confirm the presence and behavior of the PD defect based on the well-known PRPD patterns. In this specific case, since goal of the paper is to study DC partial discharge process using pulse sequences, the AC discharge raw data is also sampled in a similar manner. This is done so as to be able to generate the same set of plots that are used in the study of DC discharges.

Based on the recursive testing of several dielectric samples, it could be concluded that with increasing test voltage, all dielectric samples begin to exhibit surface discharge (when the localized tangential electrical field exceeds the breakdown field strength). The PD inception voltage and the discharge magnitude differ with different samples. However, the PRPD pattern remains similar. The PRPD pattern of surface discharge tests on the resin impregnated transformer pressboard is shown in Fig. 12. The PRPD plots have been displayed in a unipolar format to demonstrate the symmetrical discharge peaks on both voltage half-cycles. The discharge progression for the respective case, along with the plot of charge vs. voltage is shown in Fig. 13. The discharge magnitude quickly increases to very high nC levels and hence the voltage steps are limited.

The PD raw data is sampled through the externally connected oscilloscope and the pulse sequence analysis (PSA) plots are developed for the case [9]. The derived quantities of time and charge, such as difference in discharge magnitude of successive pulses (ΔQ_i and ΔQ_{i+1})and time between successive discharges (Δt_i and Δt_{i+1}) used in pulse sequence analysis (PSA) are shown in Fig. 14. The resultant PSA plots for the AC test case are shown in Fig. 15 along with a sample of the pulse stream of the discharge process. Multiple clusters are seen over the PSA plot of time between discharges (Δt_i) vs. difference in discharge

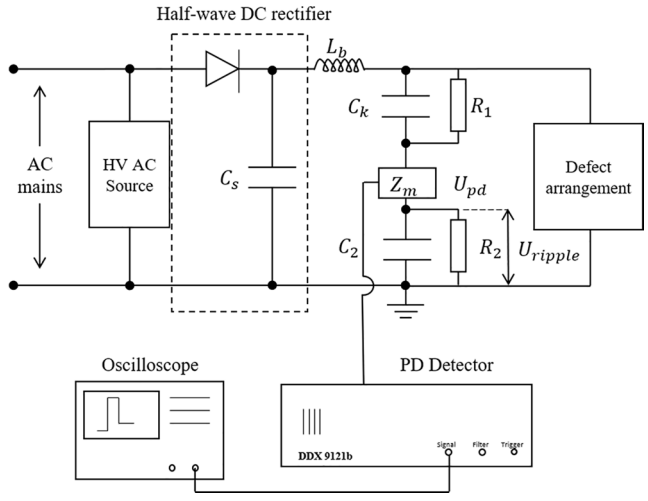

Fig. 11. Schematic of the DC-PD measuring setup according to IEC 60270 [8].

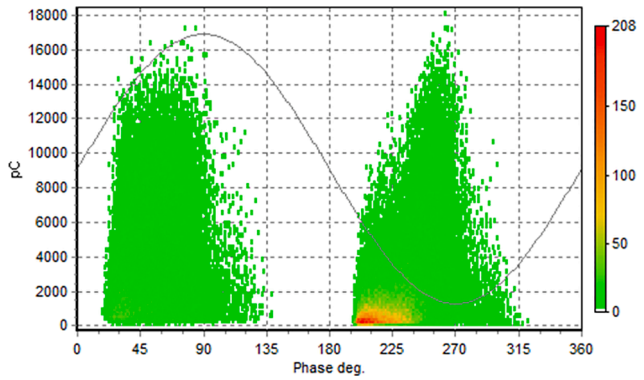

Fig. 12. The PRPD pattern of the surface discharge defect of the resin impregnated pressboard sample.

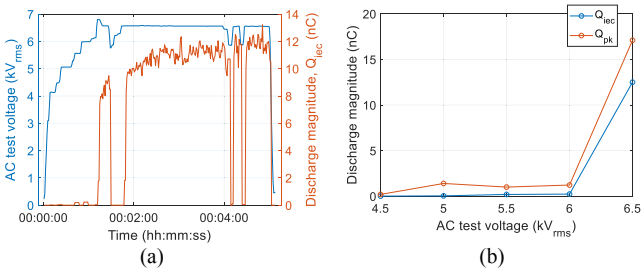

Fig. 13. (a) The discharge (PD) progression of a surface defect (sample D) and (b) the plot of charge vs. applied voltage in the respective case under AC stress.

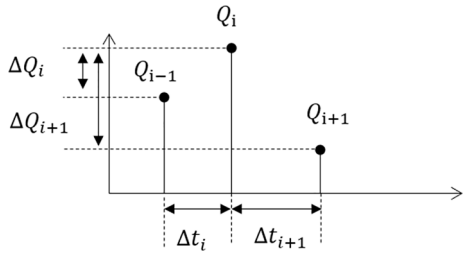

Fig. 14. An illustration of a typical PD pulse sequence acquisition showing the derived quantities of time and charge used for pulse sequence analysis (PSA), where subscript i represents the i^{th} pulse.

magnitude (ΔQ_i) and the plot of time between successive discharges (Δt_{i+1} vs. Δt_i). It can be noted that these clusters occur at a time coordinate of approximately 10 ms which can be deduced to the half-cycle period of the 50 Hz AC voltage. The absence/reduced number of pulses on the declining/falling edge of the voltage cycle or the separation between the 2 clusters on each half-cycle on the PRPD plot of Fig. 12 leads to this clustering. The PSA plots involving discharge magnitude have been developed by taking into consideration the polarity of the discharge pulse. A detailed commentary on the plots in relation to the respective DC plots is given in Section 5.

4.3. DC tests: results and observations

The DC-PD tests were performed on the different dielectric samples listed in Table 1. Not all samples exhibited surface discharge activity under DC stress. Based on the tests performed, samples A and C showed no discharge activity over the DC steady state (discharge pulses occur only during voltage ramps). Sample B shows declining PD activity, indicating a polarization current. This was also confirmed through the measurements made in Section 2, in which a slow polarization current is

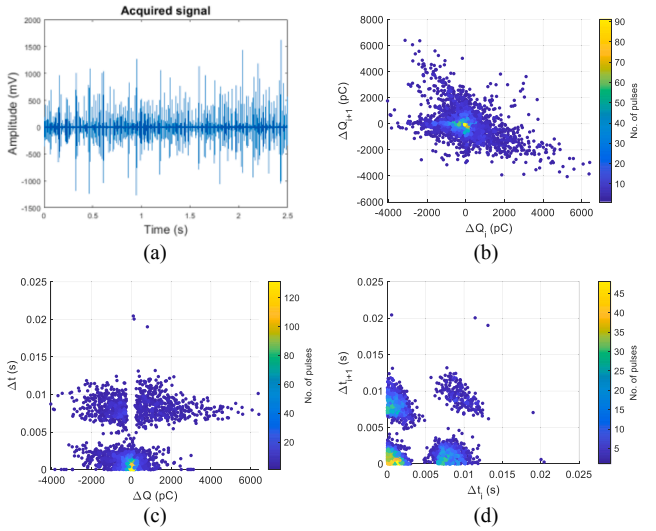

Fig. 15. The results of surface discharge measurement under AC voltage (a) pulse stream, plot of (b) ΔQ_{i+1} vs. ΔQ_i, (c) Δt_i vs. ΔQ_i and (d) Δt_{i+1} vs. Δt_i.

seen over a 30 min period. Hence, this cannot be considered as a stable and repetitive stage of discharge since the discharges fade out after the polarization phase is complete. Sample D which has the lowest electrical resistivity of them all exhibits the highest and most stable PD activity. Thus, this sample is chosen to study and understand the surface discharge process under DC with comparison to AC since it exhibits repetitive discharges with low waiting time (time lag). This section limits itself to the results of the DC-PD measurement on the resin impregnated pressboard sample.

4.3.1. Negative DC tests

The dielectric sample is stressed with negative DC voltage and the resultant pulse stream is recorded using the externally connected oscilloscope. A sample pulse stream is displayed in Fig. 16. The discharge pulses are all unipolar with a positive polarity. The discharge data is post-processed to derive the resultant pulse sequence plots as shown in Fig. 16. While investigating for visible patterns, a unique distribution is seen on the PSA plot of time between discharges, Δt_{i+1} vs. Δt_i which distinctly resembles a fish. This plot on Fig. 16(d) has been

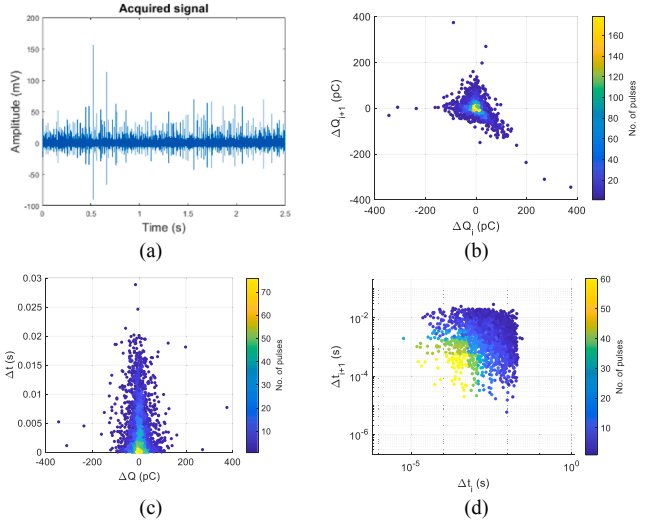

Fig. 16. The results of surface discharge measurement under negative DC voltage (a) pulse stream, plot of (b) ΔQ_{i+1} vs. ΔQ_i, (c) Δt_i vs. ΔQ_i and (d) Δt_{i+1} vs. Δt_i.

displayed on a logarithmic scale in order to visualize the distribution sufficiently.

Further, the defect progression in the respective case has been presented in Fig. 17 along with the plot of charge vs. voltage. From Fig. 17 (b), a near linear (increasing) trend in charge magnitude with increasing voltage can be observed. This is similar to the AC discharge trend, where the discharge magnitude increases with each increasing voltage step.

4.3.2. Positive DC tests

The DC-PD tests are repeated on sample D under positive DC voltage. An identical procedure as described in section 4.3.1 is followed. The results of the tests are presented in Fig. 18. The discharge pulses are all negative in polarity and the form of the PSA plots presented in Fig. 18 is similar to the ones obtained in the negative DC case. However, from Fig. 19(b) which presents the plot of charge vs. voltage it can be observed that though the discharge magnitude follows an increasing trend with increasing voltage, the rate of increase is very small. The discharge magnitude is less than 30 pC up to 25 kV_{dc}. The form of the PSA plot of time between discharges presented in Fig. 18(d) though slightly different from the negative DC case still looks uniquely distinguishable.

4.3.3. Observations on DC surface discharge

Based on the results of the DC-PD tests the following observations can be made:

i. There is a disparity in the discharge magnitude under + DC and −DC i.e. The discharge magnitude under -DC is higher than + DC.
   This phenomenon can be based on the theories of dielectric barrier discharge (DBD or surface discharge) found in literature. In [10], studying the mechanism of a single dielectric barrier plasma actuator, C.L. Enloe et al. describe the surface discharge process as quoted below;

"The DBD can maintain such a discharge because the configuration is self-limiting… To maintain a DBD discharge, an ac applied voltage is required. Fig.6a illustrates the half-cycle of the discharge for which the exposed electrode is more negative than the surface of the dielectric and the insulated electrode, thus taking the role of the cathode in the discharge. In this case, assuming the potential difference is high enough the exposed electrode can emit electrons. Because the discharge terminates on a dielectric surface, however (hence the term "dielectric barrier"), the build-up of surface charge opposes the applied voltage, and the discharge shuts itself off unless the magnitude of the applied voltage is continually increased. The behaviour of the discharge is similar on the opposite half-cycle: a positive slope in the applied voltage is necessary to maintain the discharge. In this half-cycle, the charge available to the discharge is limited to that deposited during the previous half-cycle on the dielectric surface (which now plays the role of the cathode) …"

Similarly, [11] defines the term 'back discharges' describing that the negative charges generated by the original surface discharge that propagate backwards to the electrode when the potential of the

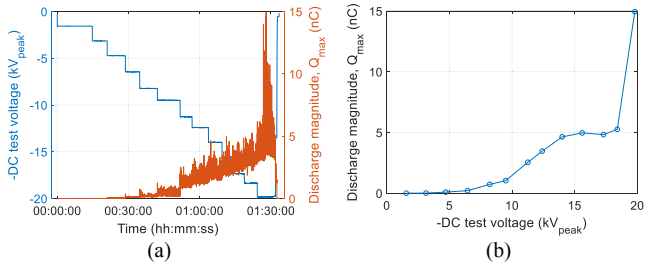

Fig. 17. (a) The discharge (PD) progression of a surface defect (sample D) and (b) the plot of charge vs. applied voltage in the respective case under negative DC stress.

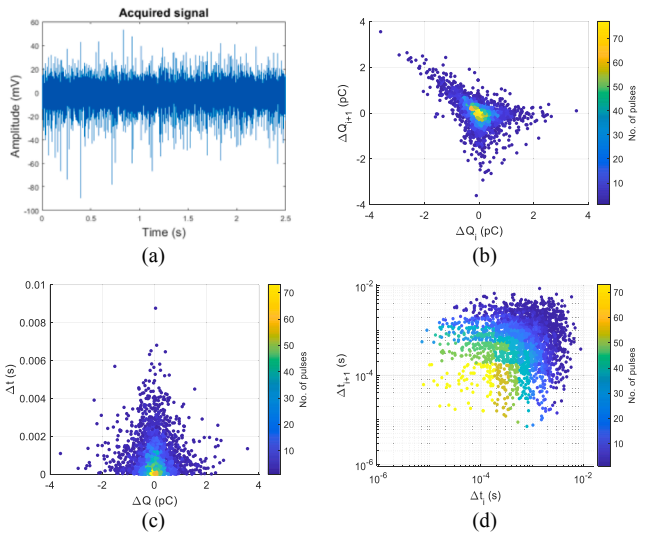

Fig. 18. The results of surface discharge measurement under positive DC voltage (a) pulse stream, plot of (b) ΔQ_{i+1} vs. ΔQ_i, (c) Δt_i vs. ΔQ_i and (d) Δt_{i+1} vs. Δt_i.

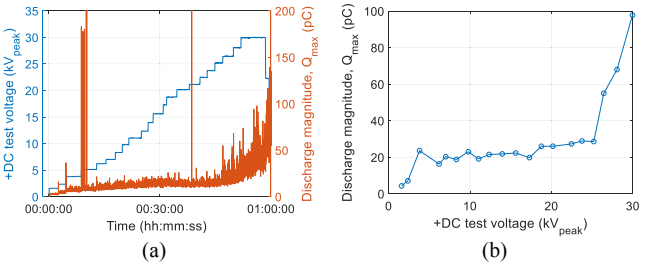

Fig. 19. (a) The discharge (PD) progression of a surface defect (sample D) and (b) the plot of charge vs. applied voltage in the respective case under positive DC stress.

electrode drops.

Therefore, based on [10,11], the actual surface discharge current is actually the electron current flowing during the negative half of the AC wave. The discharge pulses seen on the positive half is the return current arising from the electrons deposited on the surface in the previous negative half-wave. Which would explain the increased discharge magnitude in the case of -DC stress and very low discharge magnitude under + DC. The pulse recorded under + DC could even be classified as the result of impact ionization at the positive electrode instead of the surface current. Fig. 20 shows the stark difference in the charge distribution over the two voltage polarities of DC. While the same sample when tested under AC stress shows an almost similar charge distribution under both positive and negative half-cycles of the AC sine wave, as can be seen in Fig. 20.

As C.L. Enloe et al. mentions, surface discharges are self-limiting and therefore need an AC voltage to sustain. Which implies that repetitive DC discharge is only possible when the dielectric surface/interface has a higher conductivity which inhibits surface charge accumulation.

ii. Not all dielectric samples exhibit surface discharge under DC stress as they hold large surface charge which reduces the tangential component of the electrical field.

The argument made in (i) based on the self-limiting nature of the discharge is an explanation to the absence of surface PD activity in several other dielectric samples which have higher resistivities. As these samples exhibit high surface charge accumulation it limits the surface discharge activity as it opposes the applied electric field stress.

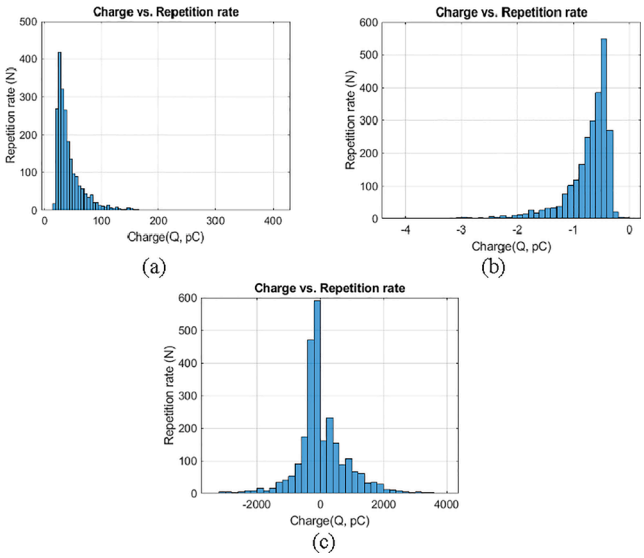

Fig. 20. Histogram of repetition rate (N) of charge (Q) for the surface discharge tests under (a) −4.7 kV_{dc} (b) + 3.8 kV_{dc} and (c) 6.5 $kV_{ac,\ RMS}$.

iii. The unique 'fish' shaped pattern in the PSA plot of time between discharges (Δt_{i+1} vs. Δt_i).

The DC surface discharge tests on the dielectric samples have revealed a distinct pattern in the plot of Δt_{i+1} vs. Δt_i which resembles closely a fish like pattern as shown in Fig. 21. Although this is a valuable visual tool in defect identification, the properties of the distribution can be explained using the WePSA (Weighted PSA) plots that were introduced in [12]. The shape of the distribution in Fig. 21 is reflected in the WePSA plot of W vs. ΔQ shown in Fig. 22 where the angle intercept between the lower (x-axis) and upper tangents gives the dispersion in the value of Δt. While the slope of the lower and upper tangent gives the value of smallest and largest values of Δt. In the case of the surface defect, the value of Δt goes from a very small value (the lower tangent almost incident with the x-axis) to a certain value of 'Δt = x'. This randomized distribution of the pulses over time is what creates the fish like pattern when translated to the PSA plot of Δt_{i+1} vs. Δt_i.

5. Similarity between ac and dc patterns

Based on the observations presented in Section 4.3.3, the surface discharge process in principle is the movement of the negative charge/electrons during the negative half-cycle in case of AC or negative polarity in case of DC. The discharge mechanism by itself is not exclusive to AC or DC. It relies on the excess tangential electrical field that causes a partial breakdown over the dielectric interface. This implies that the pulse sequence plots for the two cases should be similar if not identical

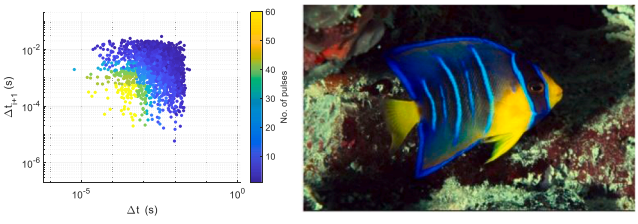

Fig. 21. The PSA plot of surface PD under -DC stress and its resemblance to an Angel fish [13].

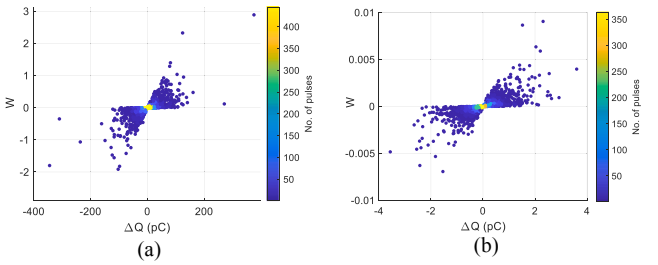

Fig. 22. The WePSA plots for surface discharge, W vs. ΔQ under (a) -DC and (b) + DC .

since the underlying physics remains the same. Therefore, this section investigates the possibility of unifying the patterns under both cases to verify the claim.

The two major inconsistencies between the AC and DC discharge stream is the clustering of the pulses over the rising edge of the voltage sine wave and its bipolar nature. To unify the two cases, the AC surface discharge raw data/ pulse stream is modified to represent a DC pulse stream. As the graphical depiction in Fig. 23 shows, the original pulse stream has discharge pulses distributed predominantly over the rising edges of the voltage wave. Firstly, the time between these two clusters on successive half-cycles is removed in step 1 through an algorithm that recognizes the last negative pulse on the positive half-wave and the first positive pulse on the negative half-wave. In step 2, all the pulses are made unipolar (with a positive polarity in this case).

The PSA plots are developed based on the modified PD data, Fig. 24 shows the resultant plots. It can be observed that the distribution becomes very similar to the DC PSA plots. This verifies the claim made in the beginning of the section that the surface discharge phenomenon in the AC and DC case are not exclusive but share the same underlying discharge process and hence still remain comparable.

6. Conclusions

This investigation on the surface discharge phenomenon under DC stress is conducted with the final goal of providing tools for defect identification under HVDC. The research approaches the problem by studying the DC defect in order to identify dominant features that are representative of the underlaying discharge mechanism rather than investigating deeply on the final patterns alone. The systematic approach to study the electrical properties of the dielectric samples under test and to later simulate the field conditions and time to DC steady state for generic cases provide valuable explanation to the observed discharge phenomenon during the PD testing phase.

The research also studies the AC surface discharge patterns not just based on its correlation/ variation with the AC sine wave (PRPD patterns) but based on the pulse sequence within each half-cycle of the voltage wave. For the DC defects with stable and repetitive discharges, the striking similarities between the AC and DC PSA patterns reveal that the surface discharge mechanism under DC stress is not exclusive but rather similar to the AC discharge process. However, additional parameters that need further investigation are the surface charge density/ holding capacity and time to steady state that heavily influence the repeatability/rate of DC-PD. Nevertheless, this paper demonstrates that in case of a measurable and repetitive surface discharge source as in the case of the resin impregnated pressboard, the DC pulse patterns resemble a unique 'fish' like pattern over the PSA plot for time between discharges (Δt_{i+1} vs. Δt_i). This unique distribution has further been explained based on the WePSA plots that were presented in [12].

During the course of the investigation, a great deal of variation with respect to the DC-PD activity was observed with various dielectric samples under study. One interesting feature that may serve as a future point of investigation is the selectivity of the dielectric sample to exhibit DC-PD activity that follows the DC ripple of the applied voltage.

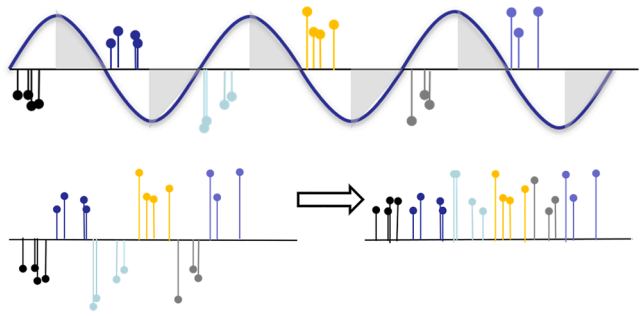

Fig. 23. (Top) A depiction of the partial discharge pulse stream over the AC voltage cycle, (below, left) the modified pulse stream by removing/ignoring the time between the voltage half-cycle with no discharge pulses and (below, right) the further modified pulse stream with unipolar pulses obtained by ignoring the pulse polarity.

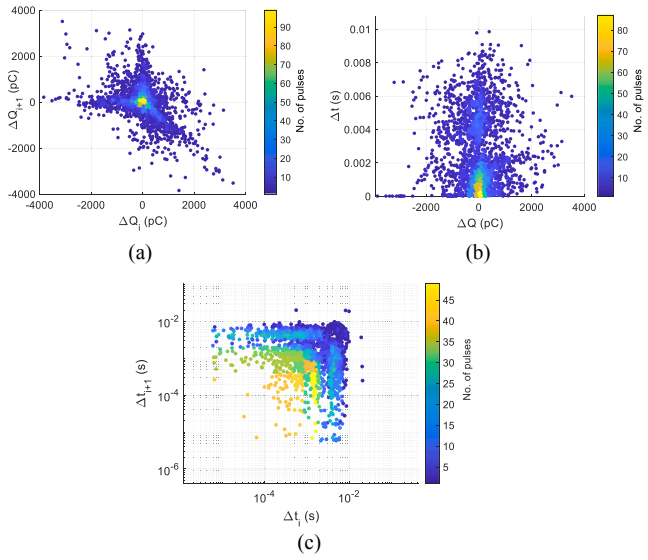

Fig. 24. The results of surface discharge measurement under AC voltage after modification of the pulse stream (a) ΔQ_{i+1} vs. ΔQ_i, (b) Δt_i vs. ΔQ_i and (c) Δt_{i+1} vs. Δt_i.

CRediT authorship contribution statement

Saliha Abdul Madhar: Conceptualization, Methodology, Formal analysis, Investigation, Writing - original draft. **Armando Rodrigo Mor:** Writing - review & editing, Supervision, Project administration. **Petr Mraz:** Writing - review & editing, Supervision. **Rob Ross:** Supervision.

Declaration of Competing Interest

The authors declare that they have no known competing financial interests or personal relationships that could have appeared to influence the work reported in this paper.

Acknowledgment

This work has partially received funding from the European Union's Horizon 2020 research and innovation programme under the Marie Sklodowska-Curie grant agreement No. 676042.

References

[1] Boggs S, Damon DH, Hjerrild J, Holboll JT, Henriksen M. Effect of insulation properties on the field grading of solid dielectric DC cable. IEEE Trans Power Deliv 2001;16(4):456–61.

[2] Christen T. Characterization and robustness of HVDC insulation. In: 2013 IEEE International conference on solid dielectrics (ICSD), Bologna; 2013. p. 238-41.

[3] Standard IEC 62631-3-1:2016. "Dielectric and resistive properties of solid insulating materials- Part 3-1: Determination of resistive properties (DC methods)-Volume resistance and volume resistivity- General method," International Electrotechnical Commission (IEC); 2016.

[4] Standard IEC 62631-3-2:2015. "Dielectric and resistive properties of solid insulating materials- Part 3-2: Determination of resistive properties (DC methods)-Surface resistance and surface resistivity," International Electrotechnical Commission (IEC); 2015.

[5] Abdul Madhar S, Brunner M, Rodrigo Mor A, Mraz P. Measurement of key dielectric properties for surface PD activity under HVDC. In: IEEE International Conference on Dielectrics, Valencia; July 2020.

[6] Comsol Multiphysics. "COMSOL Multiphysics Reference Manual," Version 5.5, 2019; p. 778-822.

[7] Seran E, Godefroy M, Pili E, Michielsen N, Bondiguel S. What we can learn from measurements of air electric conductivity in 222Rn-rich atmosphere. Earth Space Sci, 4, 91– 106, 2017.

[8] Standard IEC60270. High-voltage test techniques–Partial discharge measurements, International Electrotechnical Commission; 2000.

[9] Hoof M, Patsch R. Pulse-sequence analysis: a new method for investigating the physics of PD-induced ageing. IEE Proc – Sci Meas Technol 1995;142(1):95–101.

[10] Enloe CL, McLaughlin Thomas E, VanDyken Robert D, Kachner KD, Jumper Eric J, Cork Thomas C. Mechanisms and responses of a single dielectric barrier plasma actuator: plasma morphology. AIAA J 2004.

[11] Kumada A, Chiba M, Hidaka K. Potential distribution measurement of surface discharge by Pockels sensing technique. J Appl Phys 1998;84(6):3059–65.

[12] Abdul Madhar S, Mraz P, Rodrigo Mor A, Ross R. Empirical analysis of partial discharge data and innovative visualization tools for defect identification under DC stress. Int J Electr Power Energy Syst, Volume 123, 2020.

[13] Keywestaquarium.com, 'Most Common Fish in the Florida Keys', 2020 [Online]. Available: https://www.keywestaquarium.com/common-fish-florida-keys. [Accessed: 10- Aug – 2020].

Saliha Abdul Madhar was born in Chennai, India, in 1994. She received her MSc in Electrical Sustainable Energy with a special focus on High Voltage techniques, from the Delft University of Technology, the Netherlands, in 2017. She is currently working with HAEFELY AG in Basel, Switzerland while pursuing her PhD with the Delft University of Technology. Her PhD focusses on the study of Partial Discharge phenomenon under DC stress. Her research interests include HV Asset monitoring and diagnostics and dielectric phenomenon in HVDC.

Petr Mraz received his PhD degree in Diagnosis of Electrical Devices from the University of West Bohemia in Pilsen, Czech Republic in 2014. His research specifically focused on Partial Discharge Measurement and Evaluation. He currently works at HAEFELY AG, where he started in 2014 as an Application Engineer but has since become a Product Manager and Development Project Leader primarily responsible for Partial Discharge product line. He is a member of several CIGRE working groups and the IEC 60270 maintenance team.

Armando Rodrigo Mor is an Industrial Engineer from Universitat Politècnica de València, in Valencia, Spain, with a Ph. D. degree from this university in electrical engineering. In Spain, he joined and later led the High Voltage Laboratory and the Plasma Arc Laboratory of the Instituto de Tecnología Eléctrica in Valencia, Spain. Since 2013 he is an Assistant Professor in the Electrical Sustainable Energy Department at Delft University of Technology, in Delft, Netherlands. His research interests include monitoring and diagnostic, sensors for high voltage applications, high voltage engineering, space charge measurements and HVDC.

Robert Ross is professor at TU Delft, director of IWO (Institute for Science & Development, Ede), professor at HAN University of Applied Sciences and Asset Management Research Strategist at TenneT (TSO in the Netherlands and part of Germany). At KEMA he worked on reliability and post-failure forensic investigations. His interests concern reliability statistics, electrotechnical materials, sustainable technology and superconductivity. For energy inventions he was granted a SenterNovem Annual award and nominated Best Researcher by the World Technology Network. He recently wrote the Wiley/IEEE book "Reliability Analysis for Asset Management of Electric Power Grids" based on experience with utilities and navy.